Chiroptical properties of semiconducting nanoplatelets functionalized by tartrate derivatives

Guillaume Landaburu, Benjamin Abécassis, Benoit Fleury, Leonardo Curti

Chiroptical properties of semiconducting nanoplatelets functionalized by tartrate derivatives

Leonardo Curti,[1†‡] Guillaume Landaburu,[2‡] Benjamin Abécassis [2] and Benoit Fleury. [1*]*

[1] Sorbonne Université, CNRS, Institut Parisien de Chimie Moléculaire, IPCM, F-75005 Paris, France.

[2] ENSL, CNRS, Laboratoire de Chimie UMR 5182, 46 allée d'Italie, 69364 Lyon France

ABSTRACT

Inducing chirality in semiconductor nanoparticles is a recent trend motivated by the possible applications in circularly polarized light emission, spintronics, or stereoselective synthesis. However, the previous reports on CdSe nanoplatelets (NPLs) exclusively rely on cysteine or its derivatives as chiral ligands to induce optical activity. Here, we show a strong induction of chirality with derivatives of tartaric acid obtained by a single-step synthesis. The ligand exchange procedure in organic solvent was optimized for five-monolayer (5 ML) NPLs but can also be performed on 4 ML, 3 ML, and 2 ML. We show that the features of the CD spectra change with structural modification of the ligands and that these chiral ligands interact mainly with the first light-hole (*lh1*) band rather than the first heavy-hole (*hh1*) band, contrary to cysteine. This result suggests that chiroptical properties could be used to probe CdSe nanoplatelets' surface ligands.

KEYWORDS : CdSe, nanoplatelets, ligand exchange, surface functionalization, chirality.

INTRODUCTION

The induction of chirality in semiconducting nanocrystals, combined with their outstanding optical properties, represents a way to access a new manifold of possible applications, such as stereoselective synthesis,[1–3] chiral recognition, biosensing,[4–7] asymmetric catalysis and display devices.[8,9] Due to the large surface-to-volume ratio that characterizes nanocrystals, the coupling of chiral organic ligands with their surface has often been a method of choice to induce optical activity, as proven by the numerous examples reported in the literature for quantum dots (QDs).[9] The first reports of hybrid chiral QDs were based on thiol compounds such as cysteine, penicillamine and glutathione.[10–12] Shortly after, researchers showed that it was possible to induce optical activity in QDs with several carboxylic acids, such as maleic and tartaric acid derivatives.[13] In particular, Puri and Ferry demonstrated the interest and versatility of simple chiral carboxylic acids in the induction of chirality in semiconducting nanocrystals.[14] The authors showed that the intensity of the chiroptical activity is increased using carboxylate ligands instead of thiolates. They also showed that increasing the number of stereo-centers on the ligand using tartrate molecules can strongly enhance the dissymmetry factor. This does not apply to any other ligand since Balaz *et al.* also showed that when a second stereogenic center is added, the intensity of the CD signal of CdS QDs can either increase or decrease depending on the ligand.[15] Regarding the luminescence properties of chiral QDs, circularly polarized luminescence from cysteine stabilized QDs was first reported by the same group in 2013.[16] Nearly ten years later, Cai *et al* proposed the use of an histidine-mediated shell growth procedure, which gave CdSe/ZnS core shell QDs characterized by the highest dissymmetry factors ever reported for chiral inorganic QDs, both in absorption and luminescence.[17]

Among semiconducting nanocrystals, CdSe nanoplatelets (NPLs) do not present any size dispersion along the quantum confinement direction owing to the control of their thickness at the atomic layer scale. This peculiarity makes them suitable for very pure color displays. Therefore, the transposition of QDs-based synthetic strategies to induce chiroptical properties in NPLs appears appealing for the design of sharper optical devices. However, functionalization of such core-only NPLs by chiral ligands did not allow to keep them luminescent as described for QDs up to date. Thus, in this study we aimed to decorate CdSe NPLs with tailor-made ligands to induce chiroptic absorption properties while maintaining as sharp as possible luminescence.

In CdSe NPLs, thiol molecules largely dominate the choice of ligands to induce chirality. The first chiral CdSe NPLs report dates back to 2018, and the comprehensive work of Yang *et al.*[18] They demonstrate it is possible to induce chiroptical properties upon surface functionalization on 3, 4, and 5 ML zinc-blende (ZB) CdSe NPLs with cysteine molecules. Nevertheless, the dissymmetry g factors were found to be only slightly dependent on the platelet's thickness and in the 10^{-4} order of magnitude, as observed later by Wang *et al*.[19] The same work also studied cysteine functionalized CdSe/CdS core-shell and core-crown hetero-systems. The magnitude of the chiroptical induction was found to be inversely dependent on the thickness of the CdS shell in the core/shell system, with an almost complete quench of the chiral signal in the presence of a single layer of CdS. In contrast, in the core-crown hetero-system, the chiroptical response was not quenched but rather changed due to the summation of the CdSe and CdS contributions to the absorption. This shows that upon ligand exchange, a direct contact between the ligands and the core material is necessary for an efficient ligand-induced chirality. Another insightful work was reported by Gao *et al*.[20] In this work, the chiroptical responses of ZB and wurtzite (WZ) cysteine-functionalized NPLs were compared. The two crystal structures gave two distinct circular

dichroism signatures, and the chiroptical response's overall intensity was one order of magnitude different. These differences were attributed to the structural properties of the two different crystal phases. First, they impose different binding modes for the cysteine at the surface. Then, they are characterized by different electric dipole moments, which causes a stronger coupling between the chiral molecules and the surface cadmium cations in the case of WZ. The highest g-factor reported in this work for cysteine functionalized 3 ML WZ NPLs ($g = 5.7\times10^{-3}$ for *L*-cysteine and $g = -6.2\times10^{-3}$ for *D*-cysteine) also represents, to the best of our knowledge, the highest reported values for CdSe semiconducting nanoplatelets.[21] The second highest dissymmetry factor was reported by Kurtina *et al*[22] a year later for 2 ML ZB NPLs ($g = 3\times10^{-3}$). In this case, *N*-acetyl cysteine was used as the chiral ligand. The anomalously high dissymmetry factor (considering the crystal phase) was attributed to the coupling between the ligand-induced chirality and the intrinsic structural chirality of the nanocrystals, which were folded into nanoscrolls. In 2021, Hao and co-workers[23] obtained a cysteine functionalized CdSe/CdS system where an island-like shell of CdS was grown on native 4 ML CdSe NPLs. This heterostructure allows, at the same time, an increase of the quantum yield and the possibility for the chiral ligands to come in close contact with the CdSe core and thus produce an appreciable CD signal.

In this study, we imposed several constraints to design the chiral ligands: (*i*) thiols were not used in order to limit luminescence-quenching surface defects during ligand exchange reactions, (*ii*) alkyl chain-based ligands were chosen in order to ensure the dispersion of the nanoparticles in organic ligands and allow more chemical versatility and (*iii*) tartaric acid derivatives were used, following the work of Puri and Ferry.[14] We, therefore, present the synthesis of three different tartaric acid derivatives. The functionalization of 5 ML CdSe ZB NPLs by these ligands is described, the luminescence spectra of the resulting nanoplatelets are shown and their

chiroptical properties are discussed. In addition, the effect of such a functionalization has been studied for 2 ML, 3 ML, and 4 ML-thick NPLs.

RESULTS AND DISCUSSION

Design of chiral carboxylic acids. We hypothesized that tartaric acid derivatives would be valuable candidates to induce chirality in ZB CdSe NPLs since they present more than one stereo-center and can easily replace the initial carboxylate ligands at the NPLs surface. Furthermore, tartaric acid has been shown to induce significant CD signals on Cd-rich ZB quantum dots.[14] We choose diacetyl tartaric anhydride as a precursor for synthesizing a series of chiral carboxylic ligands able to coordinate ZB CdSe NPLs. Reacting the anhydride with a nucleophile cleaves the organic ring and generates a carboxylic function. Thus, reacting diacetyl tartaric anhydride with alcohols is a handy solution to design chiral ligands bearing variable chain lengths to address solubility issues. Starting from simple aliphatic alcohols, chiral monoesters can be obtained in one step, with high yields and without the need for cumbersome purifications.[24] Furthermore, it is possible to synthesize the desired stereoisomer since enantiopure (*R, R*) and (*S, S*) diacetyl tartaric anhydride can be purchased. We reacted both (*R, R*) and (*S, S*) diacetyl tartaric anhydride with methanol, hexan-1-ol and oleyl alcohol to produce both enantiomers of the methyl monoester of diacetyl tartaric acid (**C_1DTA**), the hexyl monoester of diacetyl tartaric acid (**C_6DTA**) and the oleyl monoester of diacetyl tartaric acid (**C_{18}DTA**) respectively (**Figure 1a**). The reaction occurs in dry dichloromethane at 40°C over 24 hours under an inert atmosphere with an excess of diacetyl tartaric anhydride with respect to the reacting alcohol (see **Figures S1 to S7** in the Supporting Information). The product of the reaction is an ester bearing the alkyl chain of the alcohol on one

side and the generated carboxylic acid on the other side, together with two asymmetric carbon atoms of the same absolute configuration as the starting diacetyl tartaric anhydride.

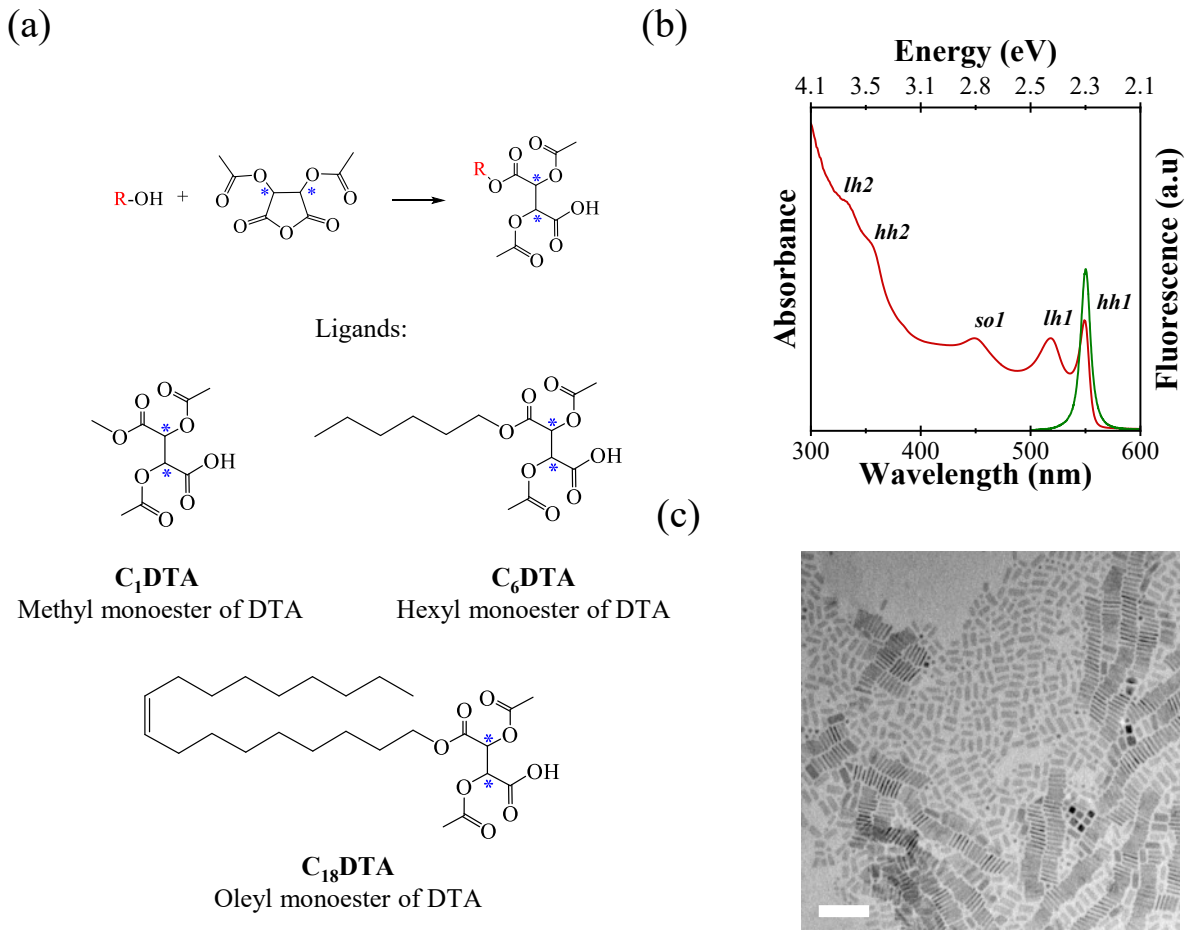

Figure 1. Synthesis of functionalized CdSe nanoplatelets (a) Chiral monoesters of DTA. Top: reaction scheme to obtain chiral monoesters of DTA, starting from diacetyl tartaric anhydride and R-OH. Bottom: chiral monoesters of DTA employed as surface ligands in this work. (b) Optical properties of native 5 ML CdSe NPLs dispersed in toluene, in red the absorption and in green the emission (λ_{exc} = 365 nm). (c) Transmission electron microscopy image showing NPLs with an average length (width) of 17.7 ± 2.8 nm (6.9 ± 1.2 nm); the scale bar corresponds to 50 nm.

The acetate/oleate-covered 5 ML CdSe NPLs synthesis has been performed as described elsewhere.[25] Briefly, cadmium oleate and selenium powder in octadecene are degassed under vacuum, put under an argon atmosphere and heated at 240 °C. Upon reaching 205 °C, cadmium acetate is added. After 10 minutes at 240 °C, oleic acid is added, and the mixture is purified by centrifugation/redispersion in a mixture of hexane and ethanol.

After purification, 5 ML CdSe NPLs are redispersed in toluene and characterized by UV-visible absorption spectroscopy, photoluminescence spectroscopy, and TEM (**Figure 1**b, c and **Figure S8** in the Supporting Information). The absorption spectrum of the as-synthesized NPLs in toluene reveals the characteristic shape of 5ML NPLs with an absorption maximum at λ = 549 nm attributed to the first heavy hole (*hh1*) excitonic transition followed by the first light hole (*lh1*) transition at λ = 518 nm and the first split-off (*so1*) transition at λ = 450 nm. In the 300-600 nm range, it is also possible to detect the second excitonic transitions at 356 nm (*hh2*) and 335 nm (*lh2*). The photoluminescence spectrum recorded in toluene with an excitation wavelength λ_{exc} = 365 nm shows a single signal at λ = 552 nm and a photoluminescence quantum yield of 28% (+/- 5%). The TEM images show that the NPLs display rectangular parallelepiped shapes with an average length of 17.7 ± 2.8 nm and a width of 6.9 ± 1.2 nm.

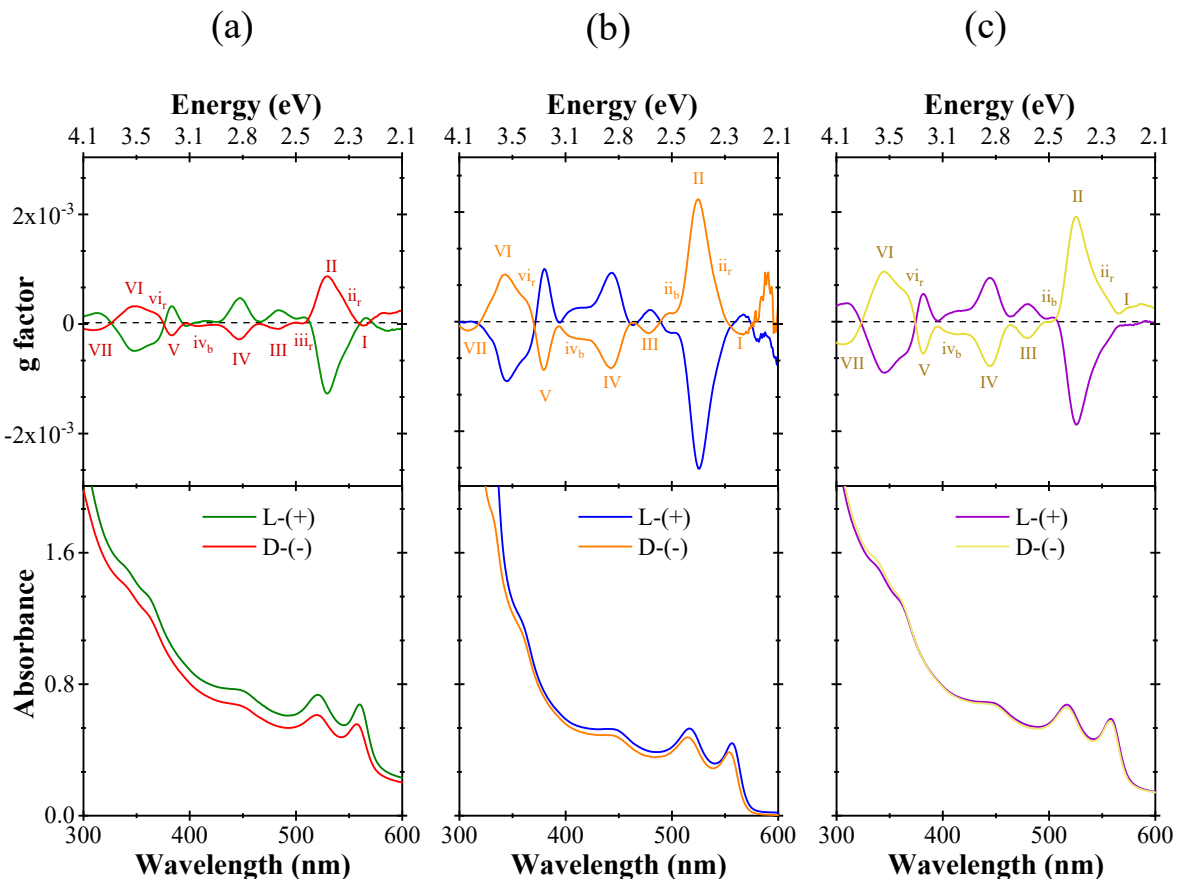

Figure 2. Absorption and g factor profiles for 5 ML nanoplatelets functionalized by both enantiomers of the chiral monoesters of diacetyl tartaric acid. Respectively by **(a)** C_1DTA, **(b)** C_6DTA, and **(c)** C_{18}DTA.

These NPLs subsequently react with the different chiral derivatives of diacetyl tartaric acid. The reaction is performed in the presence of a minimal amount of N, N-dimethylformamide (DMF) to increase the solubility of the ester in the NPL dispersion. We observed that introducing too much DMF as a cosolvent led to the degradation of the NPL, as shown by the loss of the characteristic transitions in their UV-visible spectrum. DMF can interact with surface Cd^{2+} ions as a coordinating solvent to induce their irreversible dissolution. Therefore, the amount of DMF used for the surface

ligand exchange reaction was adjusted to minimize surface degradation. Adding 20% vol. or more DMF in the mixture leads to the complete loss of the NPLs UV-VIS signal. The optimal amount was 5% vol. The exchange of native surface ligands by the chosen enantiomer of the monoester of DTA was performed initially at 60°C in this solvent mixture. The excess of chiral molecules drives the ligand exchange and occurs most likely *via* proton exchange between the bound carboxylates and the free chiral carboxylic acids in the medium.[26,27] The reaction was followed by UV-visible spectroscopy and circular dichroism (CD) until no more evolution of the optical features could be detected. At 60°C, the reaction went to completion after 48 hours. **Tables S1** to **S3** in the Supporting Information summarize the spectroscopic data recorded during the reaction optimization.

The TEM images recorded after functionalization (**Figure S10**) showed plate-like objects lying face-down on the grid, characterized by smoother edges compared to the initial system. Accordingly, the size distribution derived from the images gave a slightly reduced length of 13.7 ± 2.1 nm compared to 17.7 nm and a constant width (6.7 ± 1.3 nm) for an exchange performed at room temperature. When the exchange is performed at 60°C, the length is further reduced to 12.5 ± 2.0 nm, and the width is decreased to 5.1 ± 0.9 nm (**Figure S10**).

As can be seen from the UV-visible spectra (**Figure 2**a, b, c bottom), the ligand exchange reaction induces in all six cases *i*) an overall decrease in absorbance, *ii*) the broadening of the excitonic features, and *iii*) a redshift of some of the excitonic features. The first can be attributed, as suggested by the TEM images, to the mild erosion of the NPLs' surface, mainly due to the action of DMF and possibly to the excess of chiral carboxylates in the medium. To disentangle the two effects, we stirred the starting NPLs in the toluene/DMF mixture employed (95:5 v/v) at 60°C for 48 hours in the absence of the chiral ligands and measured a decrease of 28% of the optical

density at 400 nm (see **Figure S11**). The presence of the chiral ligands caused an additional loss comprised between 2 and 5%, which points to the DMF as the leading cause of the NPLs dissolution.

The widening and red-shift of excitonic transitions in CdSe NPLs is common when the starting stabilizing carboxylates are replaced with different ligands.[28–35] There are multiple factors contributing to this phenomenon. Since the exciton energy depends on the dielectric environment of the NPLs,[36] the broadening of the absorption features upon ligand exchange can be due to the variation of the dielectric environment of the nanocrystal core, as a result of the variation of the refractive index of the ligand brush.[37,38] Another possible factor is the partial delocalization of the carrier wave function from the NPLs to the surface ligands.[18] Finally, changes in lattice strain can also contribute to the red-shift effect.[28] If the newly introduced **C_nDTA** ligands present the same anchoring group as oleic acid, the alkyl chain is now strongly diversified with respect to a linear alkyl chain due to the presence of the acetyl side functions.

The UV-visible spectra for the particles functionalized by the **C_1DTA** and the **C_{18}DTA** display a higher baseline (**Figure 2**a, c, bottom) due to the increased scattering of the incident light. The variation of the ligand tail length affects the colloidal stability of the nanocrystals by modifying the ligand-ligand and solvent-ligand interactions.[39] The particles functionalized by **C_1DTA**, tend to aggregate due to the reduced lipophilicity of the ligand tail. The aggregation observed in the presence of **C_{18}DTA** ligand can be due to a combination of the increase in van der Waals interactions between ligand brushes, given the increased chain length, and to the depletant action exerted by the free ligands in solution (exchanged oleic acid and unreacted **C_{18}DTA**).[40,41] In both cases, the exchange results in an increased turbidity of the dispersion (**Figure S12**). In the presence of the **C_6DTA** ligand, the NPLs exhibited the optimal colloidal stability in the reaction mixture, in

line with increased colloidal stability provided by mixed ligands at the surface of CdSe quantum dots. This effect originates from an entropic gain in mixed monolayers caused by a larger number of configurations accessible by alkyl chains.[42]

The CD spectra and g factor profiles give the unambiguous confirmation of the surface functionalization of the NPLs by the chiral ligands (**Figure 2**a, b, c, top and **Figure S13** in the Supporting Information). As the CD signals arise only in correspondence with the absorption bands of the chiral species, the presence of CD bands in the visible region at the wavelengths of the excitonic transitions of the platelets is clear evidence of ligand-induced chirality. In contrast, free chiral derivatives of DTA only display a single absorption band around 200 nm (**Figure S7**), and no signal in the visible range. Similarly, the CD spectrum of the native NPLs does not present any signal in the visible range, indicating the absence of any structural chirality (**Figure S9**).

The CD bands' line shapes differ from the ones observed in chiral spherical quantum dots. In the latter case, for a given transition, the maximum in absorbance corresponds to zero CD[43] (dispersive line shape), while for NPL, the maxima in absorbance and CD occur at the same wavelength (absorptive line shapes) in line with the previous reports on cysteine functionalized CdSe NPLs.[18,20,22] The CD curves display both positive and negative Cotton effects. Spectra are opposite in sign for each enantiomer of a given ligand.

We now describe in detail the different bands of the CD spectra. We focus on the NPLs functionalized by the *D*-(-) enantiomer of the given **C_nDTA** ligand (red, orange, and yellow solid lines in **Figure 2**a, b, c, top). At first glance, the three different molecules gave almost identical chiral responses once grafted at the surface of the NPLs. One can detect in the 300-600 nm range 11 CD bands, which can be subdivided into three sets on the base of their relative intensity: strong (labeled as II, VI in **Figure 2**a, b, c, top), medium (labeled as IV, V, vi_r, VII in **Figure 2**a, b, c,

top) and weak (labeled as I, ii_r, iii_r, ii_b, III, iv_b in **Figure 2**a, c, top); in these labels, the small letters indicate shoulder peaks/dips, either blue- (b) or red- (r) shifted with respect to the absolute absorption maximum. These spectral features are fully detailed in **Tables S4**, **S5** and **S6** in the Supporting Information. A closer inspection of the CD spectra reveals that almost all the CD absorptions maintain very similar relative intensities regardless of the chiral molecules employed, except for features I and ii. Feature I appears as a low-intensity dip for the samples functionalized by **C_1DTA** and **C_6DTA** ligands, while it is almost undetectable for the sample functionalized by **C_{18}DTA**. Feature ii_r appears as a low-energy shoulder in all the cases but is more intense for the samples functionalized by the **C_1DTA** and **C_{18}DTA** ligands. These minor differences suggest that the details of the CD spectra are impacted by the conformation of the whole molecule on the surface rather than exclusively on the atoms in direct proximity to the chiral centers. This confirms previous results on spherical CdSe chiral carboxylic acid functionalized quantum dots.[13,14,44] The g factor profiles (**Figure 2**) indicate for the three different samples, that the highest dissymmetry is associated with peak II, with values comprised between 1 and 2.5×10^{-3}. This peak shows a straightforward correspondence with the *lh1* transition. If we only consider the ZB phase, previous reports gave g-factors in the 10^{-4} range (up to a maximum of 8×10^{-4}), for 3, 4 and 5 ML cysteine-functionalized NPLs,[18–20] with the only exception of the work Kurtina *et al* where 2 ML N-acetyl-cysteine-functionalized nano-scrolls allowed to reach the 10^{-3} range (3×10^{-3}).[22] Thus, the dissymmetry factors reported for C_nDTA functionalized NPLs appear to be among the highest in the literature for ZB CdSe semiconducting NPLs. These results also confirm the trend already observed for spherical quantum dots by Puri and Ferry,[14] who described a strengthening of the dissymmetry factors upon functionalisation with chiral carboxylate ligands compared to cysteine derivatives.

Effect of the temperature on ligand-exchange reaction. Given the results obtained in presence of the C_6DTA, both in terms of colloidal stability and absorption anisotropy, we pursued our study on the C_6DTA functionalized particles by exploring the effect of different reaction temperatures on the ligand-exchange reaction. To do so, 5 ML NPLs were reacted in the presence of an excess of the *D*-(-)-C_6DTA ligand at different temperatures, and the chiroptical properties were monitored for each temperature until no more evolutions were detected. The absorption, g factor profiles and CD spectra are shown in **Figure 3** and **Figure S14**.

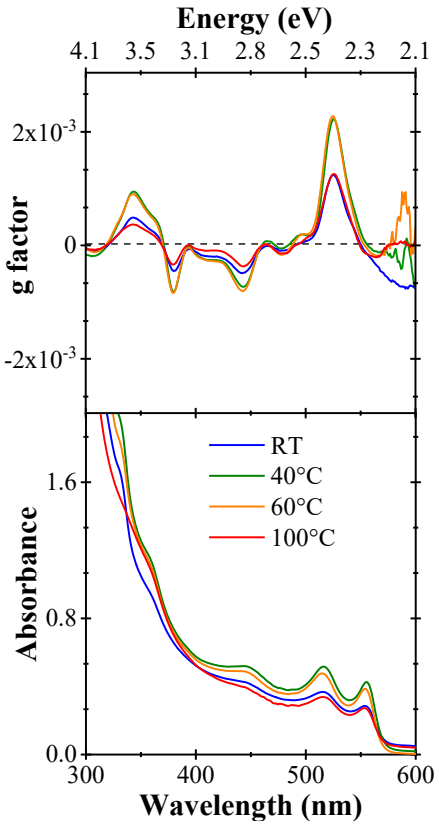

Figure 3. Absorption and g factor profiles for 5 ML NPLs reacted with the D-(-)-C_6DTA ligand at room temperature (RT), for 2 weeks (blue) at 40 °C for 96 hours (green), at 60 °C for 48 hours (orange) and at 100 °C for 24 hours (red).

We first conducted the reaction at room temperature (RT). The reaction reached the equilibrium after two weeks ($\lambda_{hh1} \approx 555$ nm), most likely because of the slow exchange kinetics. The reaction was also performed at 40 °C and 100 °C, allowing to reach equilibrium within 96 and 24 hours respectively. As shown in **Figure 3**, the different reaction temperatures affect the intensity of the g-factor profile. The ligand exchange reactions performed at 40 °C or 60 °C yield the best g-factors (about 2×10^{-3}), twice as high as those obtained at RT or 100 °C. These results suggest that the optimum temperature interval to run the ligand exchange reaction is between 40 °C and 60 °C. Higher temperature or longer reaction time cause NPLs to deteriorate as confirmed by the optical density at 400 nm.

As a consequence, we hypothesized that optimizing the ligand-exchange reaction with C_6DTA allows to restrict the creation of emission-quenching defects at the surface of the NPLs. This deleterious consequence of ligand exchange is particularly strong using thiol ligands such as cysteine. As a matter of fact, emission properties were never reported for chiral core-only nanoplatelets.[11-13] We therefore recorded the emission spectra of 5 ML NPLs after functionalization with both enantiomers of C_6DTA in toluene. Upon excitation at 365 nm, we observe in both cases the emission of the NPLs at 564 nm with a luminescence quantum yield ranging from 3% to 5% (see **Figure S15** in the Supporting Information). Although the quantum yields are moderate, this result shows that it is possible to keep the emissive properties of core-only CdSe NPLs upon ligand-exchange reactions, provided an appropriate choice of ligands and reaction conditions.

Reaction of chiral derivatives of DTA with 2, 3 and 4 ML CdSe NPLs. In order to investigate the thickness-dependence of the optical activity induced by the DTA derivatives surface functionalization, we adapted the same protocol described earlier to obtain chiral 2, 3 and 4 ML

NPLs. The CdSe NPLs of different thicknesses were synthesized as described in the experimental section. The electronic absorption spectra of these nanocrystals dispersed in toluene are given in **Figure 4** a, b, c and display typical quantum well profiles, with the first excitonic transitions gradually red-shifted as the thickness of the platelets increases (with λ_{hh1} and λ_{lh1} at 394 nm and 373 nm for 2 ML, at 463 nm and 436 for 3 ML, and at 513 nm and 481 for 4 ML). The fluorescence spectrum recorded for the 4 ML NPLs gave a narrow emission signal centered at 513 nm and characterized by a QY of 10% (+/- 5%). The TEM images showed flat rectangular plates with length of 36.0 ± 3.6 nm and width of 12.1 ± 1.7 nm for the 4 ML sample (**Figure S8**), while folded tubular structures of length 67.4 ± 10.2 nm and width 25.3 ± 4.2 nm are obtained for the 2 ML sample and extended spiral ribbons of length 389 ± 98 nm and width of 39.2 ± 8.5 nm for the 3 ML sample (**Figure S8**). The ligand exchange was, as for the 4 ML, performed by reacting a toluene/DMF (95:5 v/v) dispersion of the different NPL with the ***D*-(-)-C_6DTA** ligand, at 60 °C for 48 hours. The absorption, g factor profiles and CD spectra are given in **Figure 4** d, e, f and **Figure S16**. Analogously to what we observed with the surface functionalization of the 5 ML NPLs by the **C_6DTA** ligands, the ligand exchange red-shifts the excitonic transitions and switches the relative intensity of the first *hh* and *lh* bands. More specifically, the red-shift was found to decrease with the increase of the platelets thickness ($\Delta\lambda_{hh1}$ 2ML = 20 nm; $\Delta\lambda_{hh1}$ 3ML = 18 nm; $\Delta\lambda_{hh1}$ 4ML = 10 nm). This trend can be related to the increase of the quantum confinement going from the 4 ML system to the 2 ML system. For all NPLs thicknesses, a CD signal is observed with a similar shape shifted in wavelength: a negative Cotton effect that corresponds to the *hh1* transition and a strong positive Cotton effect at the *lh1* transition. The obtained g factors range between 7×10^{-4} to 2×10^{-3}, increasing with the thickness (**Figure 4**). Since the reaction was optimized for 5 ML NPLs, it is not surprising to see lower g-factors and absorption for other

systems. 3 ML NPLs are particularly affected as can be seen on the absorbance spectrum of the corresponding sample. 2 ML NPLs and 4 ML NPLs yield better results, with absorbances remaining higher.

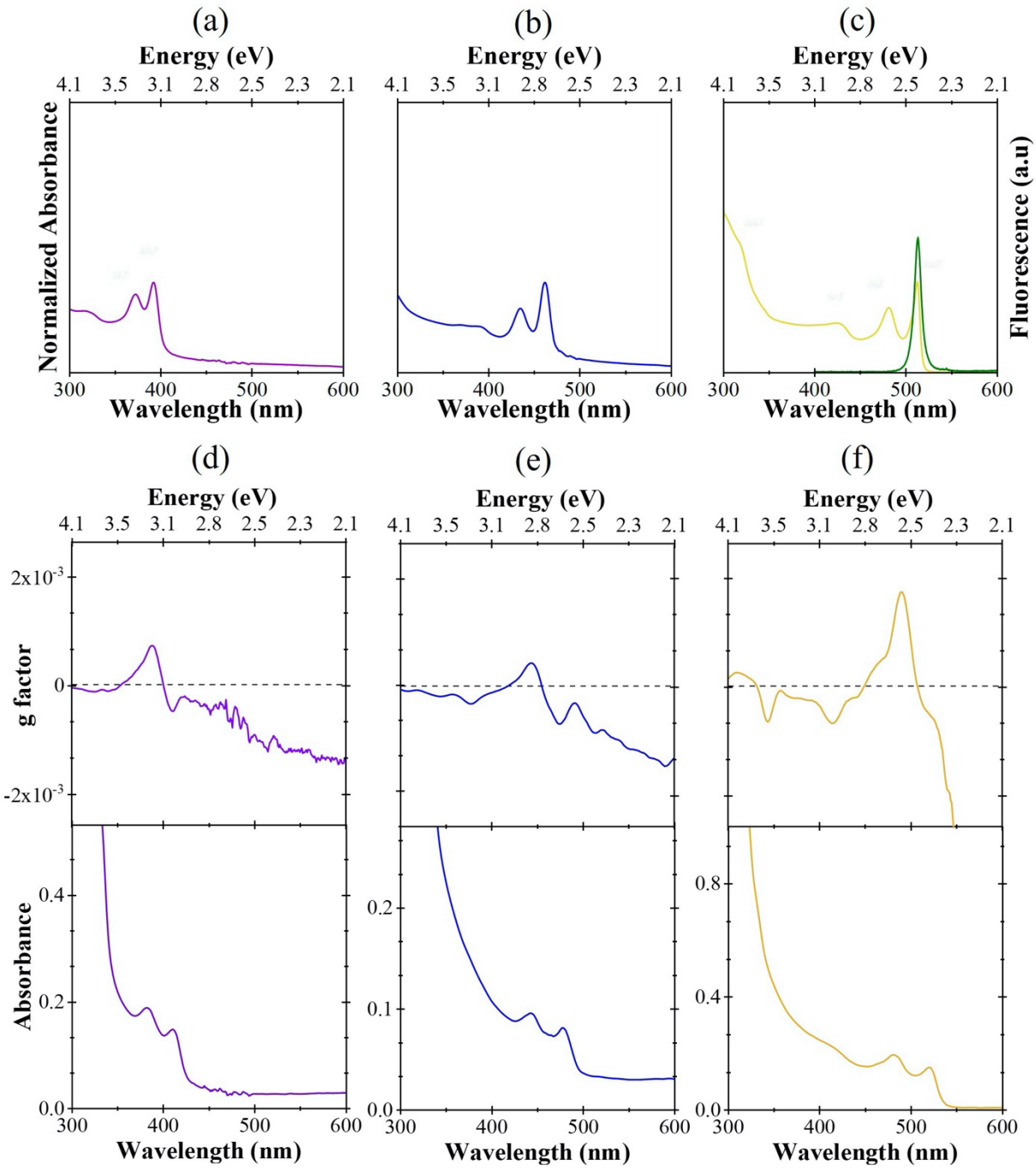

Figure 4. Optical properties of native **(a)** 2 ML, **(b)** 3 ML and **(c)** 4 ML CdSe NPLs dispersed in toluene. Absorption and g factor profiles for **(d)** 2 ML NPLs, (**e)** 3 ML NPLs and **(f)** 4 ML NPLs functionalized by D-(-)-C_6DTA ligand.

Comparison between carboxylates and thiolates. The full quantitative attribution of all the CD bands observed for the particles functionalized by the **C_nDTA** ligands would require theoretical support, and goes beyond the scope of the present work. Structural chiral distortions are known to induce optical activity in semiconductor nanocrystals, as suggested by theoretical studies.[45–47]

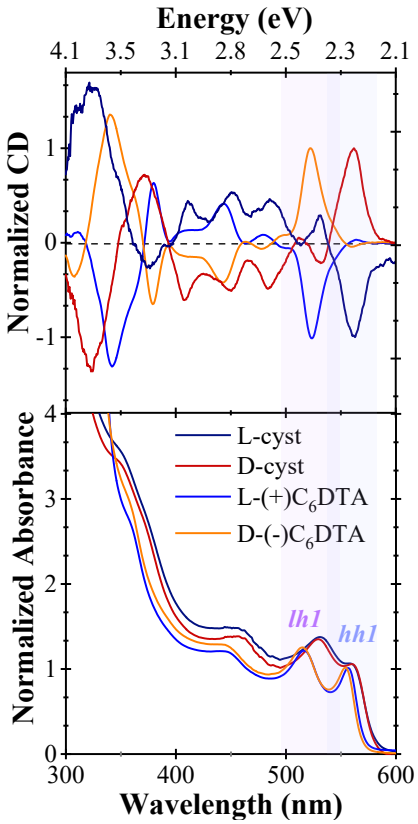

Figure 5. Normalized absorption and CD spectra of 5 ML NPLs functionalized by both enantiomers of the C_6DTA ligand and of cysteine. The spectra of the C_6DTA functionalized NPLs correspond to those in Figure 3. The cysteine spectra were obtained by ourselves after performing the ligand exchange according to the procedure reported by Yang *et al.*[18]

In first approximation, such distortions can be ruled out in the flat 5 and 4 ML, **C_nDTA** functionalized samples. Therefore, optical activity can be ascribed to the aforementioned ligand-

induced chirality. According to the work of Gao *et al*,[20] the CD spectra of CdSe NPLs functionalized by chiral cysteine molecules, can be modeled and analyzed in the framework of the so called nondegenerate coupled oscillator (NDCO) model. This model suggests that the CD signal arises from the interaction between the electric dipole transition moments of various chromophores, thus coupling the transitions of the NPLs to the transitions of their chiral surface ligands. The characteristics and orientation of the dipoles determine the magnitude and direction of the CD signal. We found interesting to compare the CD spectra obtained on the same 5 ML NPLs functionalized either with **C_nDTA** or cysteine (**Figure 5**, **Figure S17** and **Table S7** in the Supporting Information). Incidentally, CdSe NPLs functionalized by *L*(*D*)-cysteine present, in all the reported cases,[18,20] the absorption characterized by the highest dissymmetry, roughly located in correspondence with the *hh1* transition. On the other hand, the NPLs functionalized by the **C_nDTA** ligands all display the highest dissymmetry at the *lh1*. The *hh1* transition dipole is exclusively in-plane along the surface of the NPL. On the other hand, the *lh1* transition dipole is composed of both in-plane and out of plane components.[31] In the case of cysteine, the *hh1* dominant CD band indicates a coupling between the Cd-S bond acting as the ligand chromophore and the in-plane *hh1* transition dipole of the NPL.[20] Following this reasoning, the *lh1* dominant CD band in the case of **C_nDTA** ligands would result from a coupling with the out of plane component of the *lh1* transition dipole, while the near-absence of CD for the *hh1* would be due to a weak interaction with the in-plane component. This indicates a geometry in which the chromophore of **C_nDTA** ligands is almost orthogonal to the surface of the NPLs. Although theoretical simulations are required to prove this hypothesis, it appears possible to use CD spectroscopy as a tool to probe the chiral ligands conformation on the surface of the NPLs.

CONCLUSION

We report the induction of chirality in CdSe NPLs by ligand exchange with derivates of tartaric acid that can be synthesized in a single step from diacetyl tartaric anhydride, providing an easy way to implement changes to the ligand structure to tune its interaction with solvents. The ligand exchange procedure is optimized for 5 ML NPLs in organic solvent and yields high dissymmetry factors reaching up to 2.5×10^{-3}. The CD spectral features are shown to vary slightly depending on the chiral ligand structure. The ligand exchange can also be operated on 2 ML, 3 ML, and 4 ML NPLs, although the dissymmetry factor is lower in those cases. We also show that our spectra are different from those obtained by ligand exchange with cysteine, which could give insight into the ligands' orientation under the NDCO model. At last, the procedure we developed allows us to keep the luminescence of the particles.

EXPERIMENTAL SECTION

General considerations. All manipulations are performed using standard Schlenk techniques, unless otherwise indicated. All the chemicals are used as received, unless otherwise mentioned. Some of the chemicals are toxic *(e.g.* cadmium oxide and selenium), or carcinogenic (*e. g.* dichloromethane).[48] It is advised to consult the available Safety Data Sheets (SDS) provided by the producer prior to use.

Chemicals. *L-(D)*-Diacetyl tartaric anhydride (TCI, >97%), Oleyl alcohol (Alfa Aesar, 80-85%), Hexan-1-ol (Alfa Aesar, 99%), Octadecene (ODE, Acros, 90%), Oleic acid (TCI, 85%), hexane (Thermo Scientific, 97%), toluene (Fischer Chemical, 99.8%), N,N-Dimethylformamide (DMF, Acros Organics, 99.8%), sodium oleate (Sigma-Aldrich, 82%), sodium myristate (Sigma-Aldrich, 99%), Trioctylphosphine (TOP, Sigma-Aldrich, 97%), Cadmium nitrate tetrahydrate

($Cd(NO_3)_2 \cdot 4H_2O$, Sigma-Aldrich, 98%), Cadmium acetate dihydrate ($Cd(OAc)_2 \cdot 2H_2O$ Sigma-Aldrich, 98%), Selenium powder (Se, Alfa Aesar, 99.5%).

Synthesis of Cd precursors.

Cd(oleate)$_2$. In a 1 L three-neck round bottom flask equipped with an addition funnel, an inert gas inlet and a septum, 12.18 g (40 mmol, 304.44 g/mol) of sodium oleate, 200 mL EtOH 96% and 6 mL of distilled water are put under inert atmosphere and heated at 75°C using an oil bath, with vigorous stirring. After around 30 minutes, complete dissolution of the sodium oleate is achieved. In the addition funnel, a solution of 6.17 g (20 mmol, 308.48 g/mol) of $Cd(NO_3)_2 \cdot 4H_2O$ dissolved in 60 mL of EtOH 96% is loaded and introduced to the sodium oleate solution dropwise over the span of 40 minutes while still at 75°C. A white solid appears. The addition funnel is washed with 10 mL EtOH after the dropwise addition, and the reaction is let to stir at 75°C for 2-3 hours. The oil bath is removed and the reaction medium let to cool down to room temperature. It is then centrifugated at 6000 rpm (4830 RCF) for 3 minutes, the supernatant is discarded and the solid washed with hot EtOH before being centrifugated again. The washing step is performed 3 times with hot EtOH and twice with hot MeOH. The white-beige powder is recovered and lyophilized. It is advised to use the precursor within 1-2 weeks and keep it under inert atmosphere if possible.

Cd(myristate)$_2$. In a 1 L three-neck round bottom flask equipped with an addition funnel, an inert gas inlet and a septum, 1.668 g (6.66 mmol, 250.35 g/mol) of sodium myristate and 133 mL MeOH are put under inert atmosphere with vigorous stirring. After around 40 minutes, complete dissolution of the sodium myristate is achieved. In the addition funnel, a solution of 1,026 g (3.33 mmol, 308.48 g/mol) of $Cd(NO_3)_2 \cdot 4H_2O$ dissolved in 33 mL of MeOH is loaded and introduced to the sodium myristate solution dropwise over the span of 30 minutes. A white solid appears, and

when the medium gets too thick for stirring it is advised to add more MeOH (up to 500 mL can be necessary to keep the medium in motion). The reaction is let to stir at room temperature for 2 hours. The white solid is filtered using a porosity 4 glass frit. The solid is washed 3 times with cold MeOH, and the resulting paste is lyophilized. It is advised to use the precursor within 1-2 weeks and keep it under inert atmosphere if possible.

Synthesis of Se precursor.

TOP:Se. In a glovebox 1.77 g (22.4 mmol, 79,0 g/mol) of Se powder and 10 mL (22.4 mmol, 370.64 g/mol, 0.831 g/mL) of TOP are let to stir for several days until complete dissolution. This yield a 2.24 M solution of TOP:Se. It is then diluted to obtain a 1 M solution in toluene.

Synthesis of CdSe NPLs.

2 ML CdSe NPLs (adapted from Kurtina *et al*).[22] In a 50 mL three-neck round bottom flask equipped with a temperature controller, an inert gas inlet and a septum, 260.5 mg (0.977 mmol, 266.53 g/mol), 160 µL of oleic acid and 20 mL ODE are loaded. The medium is stirred and put under vacuum for about 2 hours. It is then kept under constant inert gas flux and heated to 120°C. While maintaining the temperature at 120°C, a mixture of 112 µL of TOP-Se 2.24 M solution with 138 µL of TOP and 250 µL of ODE is added, and the syringe is washed with 300 µL of ODE that are also injected into the reaction medium. The medium is kept at 120°C for 5 hours to react. 2 mL of oleic acid are added, and the medium is cooled down with a water bath. 20 mL of EtOH are added, and the whole mixture is centrifugated at 6000 rpm (4830 RCF) for 10 minutes. The precipitate is kept and redispersed in 20 mL toluene.

3 ML CdSe NPLs (adapted from Dufour *et al*).[30] In a 50 mL three-neck round bottom flask equipped with a temperature controller, an inert gas inlet and a septum, 277.5 mg (1.04 mmol, 266.53 g/mol) and 10 mL ODE are loaded. The medium is stirred and put under vacuum for about

2 hours. It is then kept under constant inert gas flux and heated to 180°C. While maintaining the temperature at 180°C, a mixture of 400 µL of TOP:Se 1 M solution with 200 µL oleic acid and 3.75 mL of ODE is added dropwise at a rate of 5mL/hour (using a syringe driver). 5 minutes after the end of the addition, 500 µL of oleic acid is added, and the medium is cooled down with a water bath. 15 mL of hexane and 15 mL of ethanol are added, and the whole mixture is centrifugated at 6000 rpm (4830 RCF) for 10 minutes. The precipitate is kept and redispersed in 20 mL toluene. If needed, adding 15 mL of ethanol and centrifugating at 6000 rpm (4830 RCF) for 10 minutes may purify remaining quantum dots. The purified NPLs are redispersed in 20 mL toluene.

4 ML CdSe NPLs. In a 50 mL three-neck round bottom flask equipped with a water cooler connected to an inert gas inlet, a temperature controller and a septum, 340 mg (0.60 mmol, 567.15 g/mol) of $Cd(myristate)_2$, 24 mg (0.30 mmol, 79,0 g/mol) of Se powder and 30 mL of ODE are loaded. The medium is stirred and kept under vacuum for about 1 hour. The flask is then kept under a constant inert gas flux, and a heating ramp of about 40°C/min is imposed until reaching a temperature of 240°C. Upon reaching 195°C during the temperature ramp (approximately 5 minutes), 80.1 mg (0.30 mmol, 266,53 g/mol) of $Cd(OAc)_2;2H_2O$ is added into the reaction medium. Upon reaching 240°C, the temperature is kept stable for 10 minutes, then 1 mL of oleic acid is added and the medium is cooled down with a water bath. It is recovered in centrifugation tubes with an addition of 20 mL hexane, and centrifugated at 6000 rpm (4830 RCF) for 10 minutes. The supernatant containing quantum dots is discarded, the precipitate is redispersed in 30 mL hexane and ethanol is added until a white veil appears. The cloudy dispersion is centrifugated at 6000 rpm (4830 RCF) for 10 minutes, the supernatant discarded and the precipitate redispersed in hexane. The process is repeated until the quantum dots are eliminated. If 3 ML NPLs are observed as a by-product, one centrifugation with only hexane as solvent should precipitate those

selectively, allowing their removal. The production of 3 ML as by-product is usually observed when the Cd(myristate)$_2$ precursor is getting too old. The final product can be redispersed in hexane or toluene, hexane being advised for long term storage. To change the solvent from hexane to toluene, the hexane is evaporated by blowing compressed air and the precipitate redispersed in toluene.

5 ML CdSe NPLs (according to Liu *et al*).[25] In a 50 mL three-neck round bottom flask equipped with a water cooler connected to an inert gas inlet, a temperature controller and a septum, 808 mg (1.20 mmol , 675.3 g/mol) of Cd(oleate)$_2$, 54 mg (0.68 mmol, 79,0 g/mol) of Se powder and 25 mL of Octadecene (ODE) are loaded. The media is stirred and kept under vacuum for about 1 hour. The flask is then kept under a constant inert gas flux, and a heating ramp of about 40°C/min is imposed until reaching a temperature of 240°C. Upon reaching 205°C during the temperature ramp (approximately 5 minutes), 208 mg (0.78 mmol, 266,53 g/mol) of Cd(OAc)$_2$·2H$_2$O is added into the reaction medium. Upon reaching 240°C, the temperature is kept stable for 10 minutes, then 1 mL of oleic acid is added and the media is cooled down with a water bath. It is recovered in centrifugation tubes with an addition of 20 mL hexane, and centrifugated at 6000 rpm (4830 RCF) for 10 minutes. The supernatant containing quantum dots is discarded, the precipitate is redispersed in 30 mL hexane and ethanol is added until a white veil appears. The cloudy dispersion is centrifugated at 6000 rpm (4830 RCF) for 10 minutes, the supernatant discarded and the precipitate redispersed in hexane. The process is repeated until the quantum dots are eliminated. The final product can be redispersed in hexane or toluene, hexane being advised for long term storage. To change the solvent from hexane to toluene, the hexane is evaporated by blowing compressed air and the precipitate redispersed in toluene.

Synthesis of C_nDTA ligand (adapted from Raghavan and Polavarapu).[24] In a 100 mL two-neck round bottom flask equipped with a septum and a condenser, L(D)-diacetyl tartaric anhydride (1 g, 4.6 mmol) is dissolved in 40 mL of dry CH_2Cl_2 under argon atmosphere. An amount (3.8 mmol) of the desired alcohol is injected. The system is heated at 40 °C for 24 hours, cooled to room temperature, and the solvent is removed under reduced pressure. The resulting crude oil is dissolved in 10 mL of $CHCl_3$ and the organic phase is extracted with HCl 0.1 M (10 mL × 5 times) to remove the unreacted anhydride. The organic phase is dried over $MgSO_4$ and the solvent removed under reduced pressure. The synthesis of the methyl monoester is performed stirring the L(D)-diacetyl tartaric anhydride in dry MeOH. The solvent is then removed by reduced pressure to obtain the pure product.

*Methyl monoester of (+)-O,O'-Diacetyl-L-tartaric acid (**L-C_1DTA**)* White solid. Yield 97 %. ($C_9H_{12}O_8$, MW: 248.2 g/mol). **^{1}H-NMR** (400 MHz, $CDCl_3$) δ 5.79 – 5.68 (m, 2H), 3.80 (s, 3H), 2.19 (d, *J* = 8.3 Hz, 6H). **^{13}C-NMR** (101 MHz, $CDCl_3$) δ 170.30, 169.92, 169.85, 166.34, 70.64, 70.39, 53.15, 20.35, 20.28.

*Methyl monoester of (-)-O,O'-Diacetyl-D-tartaric acid (**D-C_1DTA**)* White solid. Yield 98 %. ($C_9H_{12}O_8$, MW: 248.2 g/mol). **^{1}H-NMR** (400 MHz, $CDCl_3$) δ 5.75 – 5.68 (m, 2H), 3.78 (s, 3H), 2.17 (d, *J* = 8.4 Hz, 6H). **^{13}C-NMR** (101 MHz, Chloroform-*d*) δ 170.39, 169.91, 169.84, 166.33, 70.63, 70.38, 53.16, 20.35, 20.28.

*Hexyl monoester of (+)-O,O'-Diacetyl-L-tartaric acid (**L-C_6DTA**)* Transparent viscous oil. Yield: 89 % ($C_{14}H_{22}O_8$, MW: 318.3 g/mol). **^{1}H-NMR** (400 MHz, $CDCl_3$) δ 5.75 (d, *J* = 2.6 Hz, 1H), 5.71 (d, *J* = 2.7 Hz, 1H), 5.42 (s, 1H), 4.27 – 4.10 (m, 2H), 2.19 (s, 3H), 2.16 (s, 3H), 1.68 – 1.54 (m, 2H), 1.37 – 1.22 (m, 6H), 0.89 (t, 3H). **^{13}C NMR** (101 MHz, $CDCl_3$) δ 170.68, 169.77,

169.64, 165.77, 70.66, 70.42, 66.54, 31.28, 28.37, 25.31, 22.46, 20.37, 20.25, 13.95. CD (MeOH 1 mM) λ/*g-factor*: 228/-2.6×10^{-2}.

*Hexyl monoester of (-)-O,O'-Diacetyl-L-tartaric acid (**D-C_6DTA**)* Whitish viscous oil. Yield: 92 % ($C_{14}H_{22}O_8$, MW: 318.3 g/mol). **^{1}H NMR** (400 MHz, $CDCl_3$) δ 6.18 (s, 1H), 5.75 (d, *J* = 2.7 Hz, 1H), 5.71 (d, *J* = 2.7 Hz, 1H), 4.27 – 4.09 (m, 2H), 2.19 (s, 3H), 2.16 (s, 3H), 1.68 – 1.54 (m, 2H), 1.37 – 1.22 (m, 6H), 0.88 (t, 3H). **^{13}C NMR** (101 MHz, $CDCl_3$) δ 170.60, 169.79, 169.66, 165.79, 70.67, 70.43, 66.54, 31.28, 28.37, 25.30, 22.46, 20.36, 20.25, 13.95. CD (MeOH 1 mM) λ/*g-factor*: 228/-2.3×10^{-2}.

*Oleyl monoester of (+)-O,O'-Diacetyl-L-tartaric acid (**L-C_{18}DTA**)*: Pale yellow viscous oil. Yield: 85 % ($C_{26}H_{44}O_8$, MW: 484.6 g/mol). **^{1}H NMR** (400 MHz, $CDCl_3$) δ 5.76 (d, *J* = 2.7 Hz, 1H), 5.71 (d, *J* = 2.7 Hz, 1H), 5.45 – 5.29 (m, 2H), 4.35 – 3.99 (m, 2H), 2.19 (s, 3H), 2.17 (s, 3H), 2.10 – 1.88 (m, 4H), 1.74 – 1.52 (m, 2H), 1.48 – 1.16 (m, 22H), 0.88 (t, 3H). **^{13}C NMR** (101 MHz, $CDCl_3$) δ 169.95, 169.86, 169.80, 165.92, 129.99, 129.73, 70.74, 70.52, 66.53, 31.89, 29.75, 29.71, 29.64, 29.50, 29.36, 29.30, 29.20, 29.11, 28.41, 27.20, 27.17, 25.62, 22.66, 20.33, 20.25, 14.09. CD (hexane 1 mM) *λ/g-factor*: 215/- 4.2×10^{-3}.

*Oleyl monoester of (-)-O,O'-Diacetyl-D-tartaric acid, (**D-C_{18}DTA**):* Pale yellow viscous oil. Yield: 88 %. ($C_{26}H_{44}O_8$, MW: 484.6 g/mol). **^{1}H NMR** (400 MHz, CDCl3) δ 5.76 (d, *J* = 2.7 Hz, 1H), 5.71 (d, *J* = 2.7 Hz, 1H), 5.42 – 5.26 (m, 2H), 4.33 – 4.06 (m, 2H), 2.19 (s, 3H), 2.17 (s, 3H), 2.10 – 1.90 (m, 4H), 1.76 – 1.51 (m, 2H), 1.42 – 1.16 (m, 22H), 0.88 (t, 3H). **^{13}C NMR** (101 MHz, $CDCl_3$) δ 169.98, 169.81, 169.77, 165.94, 129.97, 129.72, 70.74, 70.52, 66.53, 31.88, 29.73, 29.70, 29.62, 29.49, 29.35, 29.29, 29.19, 29.10, 28.39, 27.19, 27.16, 25.62, 22.65, 20.30, 20.23, 14.07. 215/+6×10^{-3}.

Ligand exchange. In a 4 mL vial with a stirring bar, 0.126 mmol of **C_nDTA** ligand are dissolved in 100 µL of DMF and 900 µL of toluene. A solution of 5 ML NPLs in toluene is diluted to an absorbance of 2 at the *hh1* peak. 1 mL of the NPLs solution is added to the vial containing the **C_nDTA** ligand solution. The mixture is left to stir in an oil bath at 60 °C for 48 hours.

Absorption spectroscopy. Absorbance spectra for NPLs without chiral ligands were obtained on a Perkin-Elmer Lambda 750 (2ML and 3ML) or a Jasco V730 (4ML and 5ML) spectrometer using 1 cm quartz cuvettes. Samples were diluted in toluene to reach an optical density of 0.5 at the *hh1* absorption peak.

Circular dichroism (CD) spectroscopy. CD spectra were collected on a J-1700. During the measurement the CD signal (mdeg), the tension (V) and the absorption were collected simultaneously on three separate channels. The samples were measured using a 1 cm quartz cell, 2 seconds digital integration time (D.I.T), 1.0 nm bandwidth, a data pitch of 0.5 nm and a scanning speed of 200 nm/min. Each spectrum is the average of 3 accumulations. The dissymmetry factors (g factors) reported in the text were calculated using the values of absorbance simultaneously measured during the CD measurement, according to the equation g factor = CD / (32980 × Abs). The g factor is dimensionless and allows to compare chiroptical activity across various chiral systems.

Fluorescence spectroscopy. Fluorescence spectra were obtained on a Fluorolog Horiba Jobin Yvon. For qualitative measurement of the fluorescence spectrum profile, 1 cm quartz cuvettes can be used. For the quantum yield measurement, an integrating sphere and quartz NMR tube are used. Irradiation was set at 365 nm for 5 ML. Samples were diluted in toluene to reach an optical density below 0.1 at the *hh1* absorption peak.

Nuclear magnetic resonance (NMR) spectroscopy. ^{1}H and ^{13}C NMR spectra are measured on Bruker spectrometers (Avance II 300 MHz, equipped with a QNP probe, Avance III 300 et 400

MHz Nanobay, equipped with a BBFO probe), with 5 mm tubes. The reference for ^{1}H and ^{13}C NMR spectra is the tetramethylsilane signal. The solvent is used as an internal reference. Chemical shifts, δ, are expressed in parts per millions (ppm) and are referenced using IUPAC recommendations.[49] The data were treated using the software MestreNova.[50]

Transmission electron microscopy (TEM). TEM imagery was performed on a JEOL JEM1400 under the voltage of 100kV. TEM grids were prepared by stirring vigorously the sample and depositing a 10µL drop on the grid before letting it to dry overnight.

ACKNOWLEDGEMENTS

This article is part of a project that has received funding from the European Research Council (ERC CoG SENECA) under the European Union's Horizon 2020 research and innovation programme (Grant agreement No. 865995). We thank Elisabeth Errazuriz-Cerda and Bruno Chapuis from the Centre d'Imagerie Quantitative Lyon 1 for allowing us access to the JEOL JEM1400.

ASSOCIATED CONTENT

Supporting Information.

The following files are available free of charge.

C_nDTA ligands characterization: ^{1}H and ^{13}C-NMR spectra, Absorption and CD spectra

CdSe NPLs before ligand exchange: TEM images of CdSe NPLs before ligand exchange, Absorption and CD spectra of CdSe NPLs before ligand exchange

Optimization of surface ligands exchange conditions

TEM images of CdSe NPLs functionalized by C_6DTA ligands

Effect of DMF on optical features in ligand-exchange conditions

Aspect of 5 ML NPLs dispersions after ligand exchange

Spectral features of 5 ML CdSe NPLs after ligand exchange with C_nDTA ligands

Emission spectra of 5 ML CdSe NPLs before and after functionalization with C_6DTA

Spectral features of 2, 3, 4 ML CdSe NPLs after ligand exchange with C_nDTA ligands

Spectral features of 5 ML CdSe NPLs after ligand exchange with cysteine

AUTHOR INFORMATION

Corresponding Author

*E-mail: benjamin.abecassis@ens-lyon.fr; benoit.fleury@sorbonne-universite.fr

Present Addresses

†Laboratoire de Physique et d'Etude des Matériaux, ESPCI-Paris, PSL Research University, Sorbonne Université Univ Paris 06, CNRS UMR 8213, 10 rue Vauquelin 75005 Paris, France.

Author Contributions

The manuscript was written through contributions of all authors. All authors have given approval to the final version of the manuscript. ‡These authors contributed equally.

REFERENCES

(1) Berova, N.; Bari, L. D.; Pescitelli, G. *Chem. Soc. Rev.* **2007**, *36*, 914.

(2) Ben-Moshe, A.; Maoz, B. M.; Govorov, A. O.; Markovich, G. *Chem. Soc. Rev.* **2013**, *42*, 7028–7041.
(3) Milton, F. P.; Govan, J.; Mukhina, M. V.; Gun'ko, Y. K. *Nanoscale Horiz.* **2015**, *1*, 14–26.
(4) Yoo, S.; Park, Q.-H. *Nanophotonics* **2019**, *8*, 249–261.
(5) Mejía-Salazar, J. R.; Oliveira, O. N. Jr. *Chem. Rev.* **2018**, *118*, 10617–10625.
(6) A. Paiva-Marques, W.; Reyes Gómez, F.; N. Oliveira, O.; Mejía-Salazar, J. R. *Sensors* **2020**, *20*, 944.
(7) Lee, Y. Y.; Kim, R. M.; Im, S. W.; Balamurugan, M.; Nam, K. T. *Nanoscale* **2019**, *12*, 58–66.
(8) Liu, J.; Yang, L.; Qin, P.; Zhang, S.; Yung, K. K. L.; Huang, Z. *Adv. Mater.* **2021**, *33*, 2005506.
(9) Kuznetsova, V.; Gromova, Y.; Martinez-Carmona, M.; Purcell-Milton, F.; Ushakova, E.; Cherevkov, S.; Maslov, V.; Gun'ko, Y. K. *Nanophotonics* **2021**, *10*, 797–824.
(10) Moloney, M. P.; Gun'ko, Y. K.; Kelly, J. M. *Chem. Commun.* **2007**, No. 38, 3900.
(11) Bloom, B. P.; Kiran, V.; Varade, V.; Naaman, R.; Waldeck, David. H. *Nano Lett.* **2016**, *16*, 4583–4589.
(12) Kuznetsova, V. A.; Visheratina, A. K.; Ryan, A.; Martynenko, I. V.; Loudon, A.; Maguire, C. M.; Purcell-Milton, F.; Orlova, A. O.; Baranov, A. V.; Fedorov, A. V.; Prina-Mello, A.; Volkov, Y.; Gun'Ko, Y. K. *Chirality* **2017**, *29*, 403–408.
(13) Varga, K.; Tannir, S.; Haynie, B. E.; Leonard, B. M.; Dzyuba, S. V.; Kubelka, J.; Balaz, M. *ACS Nano* **2017**, *11*, 9846–9853.
(14) Puri, M.; Ferry, V. E. *ACS Nano* **2017**, *11*, 12240–12246.
(15) Joh, Y. A.; Kwon, Y. H.; Tannir, S.; Leonard, B. M.; Kubelka, J.; Varga, K.; Balaz, M. *J. Mater. Chem. C* **2021**, *9*, 17483–17495.
(16) Tohgha, U.; Deol, K. K.; Porter, A. G.; Bartko, S. G.; Choi, J. K.; Leonard, B. M.; Varga, K.; Kubelka, J.; Muller, G.; Balaz, M. *ACS Nano* **2013**, *7*, 11094–11102.
(17) Cai, J.; Liu, A.-A.; Shi, X.-H.; Fu, H.; Zhao, W.; Xu, L.; Kuang, H.; Xu, C.; Pang, D.-W. *J. Am. Chem. Soc.* **2023**, *145*, 24375–24385.
(18) Yang, G.; Kazes, M.; Oron, D. *Adv. Funct. Mater.* **2018**, *28*, 1802012.
(19) Wang, X.; Hao, J.; Cheng, J.; Li, J.; Miao, J.; Li, R.; Li, Y.; Li, J.; Liu, Y.; Zhu, X.; Liu, Y.; Sun, X. W.; Tang, Z.; Delville, M.-H.; He, T.; Chen, R. *Nanoscale* **2019**, *11*, 9327–9334.
(20) Gao, X.; Zhang, X.; Zhao, L.; Huang, P.; Han, B.; Lv, J.; Qiu, X.; Wei, S.-H.; Tang, Z. *Nano Lett.* **2018**, *18*, 6665–6671.
(21) Ma, W.; Xu, L.; de Moura, A. F.; Wu, X.; Kuang, H.; Xu, C.; Kotov, N. A. *Chem. Rev.* **2017**, *117*, 8041–8093.
(22) Kurtina, D. A.; Garshev, A. V.; Vasil'eva, I. S.; Shubin, V. V.; Gaskov, A. M.; Vasiliev, R. B. *Chem. Mater.* **2019**, *31*, 9652–9663.
(23) Hao, J.; Zhao, F.; Wang, Q.; Lin, J.; Chen, P.; Li, J.; Zhang, D.; Chen, M.; Liu, P.; Delville, M.-H.; He, T.; Cheng, J.; Li, Y. *Adv. Opt. Mater.* **2021**, *9*, 2101142.
(24) Raghavan, V.; Polavarapu, P. L. *J. Phys. Chem. B* **2017**, *121*, 1629–1639.
(25) Liu, J.; Guillemeney, L.; Abécassis, B.; Coolen, L. *Nano Lett.* **2020**, *20*, 3465–3470.
(26) De Nolf, K.; Cosseddu, S. M.; Jasieniak, J. J.; Drijvers, E.; Martins, J. C.; Infante, I.; Hens, Z. *J. Am. Chem. Soc.* **2017**, *139*, 3456–3464.
(27) Fritzinger, B.; Capek, R. K.; Lambert, K.; Martins, J. C.; Hens, Z. *J. Am. Chem. Soc.* **2010**, *132*, 10195–10201.

(28) Antanovich, A.; Achtstein, A. W.; Matsukovich, A.; Prudnikau, A.; Bhaskar, P.; Gurin, V.; Molinari, M.; Artemyev, M. *Nanoscale* **2017**, *9*, 18042–18053.
(29) Diroll, B. T. *Chem. Mater.* **2020**, *32*, 5916–5923.
(30) Dufour, M.; Qu, J.; Greboval, C.; Méthivier, C.; Lhuillier, E.; Ithurria, S. *ACS Nano* **2019**, *13*, 5326–5334.
(31) Diroll, B. T.; Schaller, R. D. *Chem. Mater.* **2019**, *31*, 3556–3563.
(32) Wang, F.; Wang, Y.; Liu, Y.-H.; Morrison, P. J.; Loomis, R. A.; Buhro, W. E. *Acc. Chem. Res.* **2015**, *48*, 13–21.
(33) Zhou, Y.; Buhro, W. E. *J. Am. Chem. Soc.* **2017**, *139*, 12887–12890.
(34) Sun, H.; Buhro, W. E. *Chem. Mater.* **2020**, *32*, 5814–5826.
(35) Yao, Y.; DeKoster, G. T.; Buhro, W. E. *Chem. Mater.* **2019**.
(36) Shin, A. J.; Hossain, A. A.; Tenney, S. M.; Tan, X.; Tan, L. A.; Foley, J. J.; Atallah, T. L.; Caram, J. R. *J. Phys. Chem. Lett.* **2021**, *12*, 4958–4964.
(37) Diroll, B. T.; Gaulding, E. A.; Kagan, C. R.; Murray, C. B. *Chem. Mater.* **2015**, *27*, 6463–6469.
(38) Chehaibou, B.; Izquierdo, E.; Chu, A.; Abadie, C.; Cavallo, M.; Khalili, A.; Dang, T. H.; Gréboval, C.; Xu, X. Z.; Ithurria, S.; Vincent, G.; Gallas, B.; Mugny, G.; Arnaud, A.; Lhuillier, E.; Delerue, C. *Nanoscale* **2022**, *14*, 2711–2721.
(39) Calvin, J. J.; Brewer, A. S.; Alivisatos, A. P. *Nat. Synth.* **2022**, *1*, 127–137.
(40) Lekkerkerker, H. N. W.; Tuinier, R. *Colloids and the Depletion Interaction*; Lecture Notes in Physics; Springer Netherlands: Dordrecht, 2011; Vol. 833.
(41) Jana, S.; Phan, T. N. T.; Bouet, C.; Tessier, M. D.; Davidson, P.; Dubertret, B.; Abécassis, B. *Langmuir* **2015**, *31*, 10532–10539.
(42) Pang, Z.; Zhang, J.; Cao, W.; Kong, X.; Peng, X. *Nat. Commun.* **2019**, *10*, 2454.
(43) Ben-Moshe, A.; Teitelboim, A.; Oron, D.; Markovich, G. *Nano Lett.* **2016**, *16*, 7467–7473.
(44) Wu, Y.; Shao, X.; Zhou, Y.; Jiang, S.; Zhang, T.; Yan, Y. *Nanotechnology* **2021**, *32*, 375701.
(45) Tepliakov, N. V.; Baimuratov, A. S.; Vovk, I. A.; Leonov, M. Yu.; Baranov, A. V.; Fedorov, A. V.; Rukhlenko, I. D. *ACS Nano* **2017**, *11*, 7508–7515.
(46) Baimuratov, A. S.; Gun'ko, Y. K.; Shalkovskiy, A. G.; Baranov, A. V.; Fedorov, A. V.; Rukhlenko, I. D. *Adv. Opt. Mater.* **2017**, *5*, 1600982.
(47) Baimuratov, A. S.; Pereziabova, T. P.; Leonov, M. Yu.; Zhu, W.; Baranov, A. V.; Fedorov, A. V.; Gun'ko, Y. K.; Rukhlenko, I. D. *ACS Nano* **2018**, *12*, 6203–6209.
(48) Vidal, S. *ACS Cent. Sci.* **2020**, *6*, 83–86.
(49) Harris, R. K.; Becker, E. D.; Cabral de Menezes, S. M.; Goodfellow, R.; Granger, P. *Pure Appl. Chem.* **2001**, *73*, 1795–1818.
(50) Claridge, T. *J. Chem. Inf. Model.* **2009**, *49*, 1136–1137.